Electrochimica Acta 487 (2024) 144200

Contents lists available at ScienceDirect

Electrochimica Acta

journal homepage: www.journals.elsevier.com/electrochimica-acta

Towards improved online dissolution evaluation of Pt-alloy PEMFC electrocatalysts via electrochemical flow cell - ICP-MS setup upgrades

Leonard Moriau [a], Tina Đukić [a,b], Vojtech Domin [c], Roman Kodym [c], Martin Prokop [c], Karel Bouzek [c], Matija Gatalo [a,d], Martin Šala [e,*], Nejc Hodnik [a,f,**]

[a] Department of Materials Chemistry, National Institute of Chemistry, Hajdrihova Ulica 19, 1000 Ljubljana, Slovenia
[b] Faculty of Chemistry and Chemical Technology, University of Ljubljana, Večna pot 113, 1000 Ljubljana, Slovenia
[c] Deparment of Inorganic Technology, University of Chemistry and Technology, Technicka 5, 166 28 Prague 6, Czech Republic
[d] ReCatalyst d.o.o., Hajdrihova Ulica 19, 1000 Ljubljana, Slovenia
[e] Department of Analytical Chemistry, National Institute of Chemistry, Hajdrihova Ulica 19, 1000 Ljubljana, Slovenia
[f] University of Nova Gorica, 5000 Nova Gorica, Slovenia

ARTICLE INFO

Keywords:
Fuel cell catalyst
Pt-alloys dissolution
Online-ICP-MS
Electrocatalysis
Flow injection analysis

ABSTRACT

Electrochemical flow cell coupled with an inductively coupled plasma mass spectrometer (EFC-ICP-MS) is a powerful electroanalytical technique to monitor *in-situ* dissolution of metallic electrocatalysts and to understand mechanism of degradation under operating conditions. Its utilisation has witnessed a notable increase in the electrocatalyst field in the last decade where it has been extensively used to study the stability of platinum group metals (PGMs) under oxygen reduction and oxygen evolution reaction conditions. Online ICP-MS has allowed the scientific and industrial community to optimise the activity and stability of PGMs thanks to a better understanding of the complex metal corrosion processes. Among the different setups, the electrochemical flow cell design is the most common as it is based on a commercially available design. Nonetheless, besides different materials and different electrochemical protocols, the impact of the geometry and various parameters of the setup on the recorded dissolution signal has not been studied until now. Such parameters can influence the results obtained with an EFC-ICP-MS and thus the interpretation of the dissolution mechanism and/or stability assessment. Hereby, we demonstrate that the length of the tubing between the outlet of the cell and the inlet of the ICP-MS impacts the resolution of the PtCo catalyst dissolution peaks. This, in turn, facilitates studies where the detection of extremely low concentrations is necessary, such as under a very narrow potential window. Similarly, a reduced internal volume of the cell restricts Pt redeposition, contributing to a more precise evaluation of stability. These claims were supported by dynamic continuum mechanics modelling of the ion concentration in a model EFC. Finally, we provide guidelines and advice to properly measure dissolution with an electrochemical cell coupled with ICP-MS.

1. Introduction

Proton exchange membrane fuel cell (PEMFC) is an increasingly important technology in the transition from fossil-fuel energy to a green, hydrogen-based economy [1,2]. This technology has the potential to provide zero-emission chemical energy by combining hydrogen and oxygen [3]. Unfortunately, the high cost of the Pt catalysts, needed to catalyse the sluggish oxygen reduction reaction (ORR), has hindered the commercialisation of PEMFC [4,5]. The implementation of a new generations of Pt-alloy catalysts has notably brought the price down by replacing the previously unused Pt from the core of nanoparticles with transition metals (M = Co, Cu, Ni or Fe) and consequently diminished the amount of precious metal required [6–11]. In addition, "core-shell" and or "de-alloyed Pt alloys" (Pt-M) nanoparticles exhibit better intrinsic activity than pure Pt surface due to ligand and/or strain effect [12,13].

However, a new challenge has arisen for the Pt-alloys catalysts due to the intrinsically lower stability of transition metals [1,14-17]. The dissolved transition metal ions can decrease the performance of PEMFC by

* Corresponding author at: M. Šala: Department of Analytical Chemistry, National Institute of Chemistry, 1000 Ljubljana, Slovenia.
** N. Hodnik: Department of Materials Chemistry, National Institute of Chemistry, 1000 Ljubljana, Slovenia; University of Nova Gorica, 5000 Nova Gorica, Slovenia.
E-mail addresses: martin.sala@ki.si (M. Šala), nejc.hodnik@ki.si (N. Hodnik).

https://doi.org/10.1016/j.electacta.2024.144200
Received 18 January 2024; Received in revised form 27 March 2024; Accepted 30 March 2024
Available online 2 April 2024

blocking the Pt surface, depositing in the ionomer [18,19] and hindering the mass transport within [20], or catalysing unwanted reactions in the membrane [21]. Hence, improving the stability of Pt-alloys should be achieved based on a thorough fundamental understanding of its dissolution behaviour.

One possible way to study the parameters influencing the stability of Pt-M catalysts is to utilise an electrochemical cell connected to an inductively coupled plasma mass spectrometry (ICP-MS) [22–25]. It allows online monitoring of the concentration of the dissolved metals and thus directly correlating it to the operating conditions. This technique is extremely versatile and sensitive, with a detection limit in the range of part per trillion, while often used for ppb detection. It has been shown effective in revealing mechanisms of dissolution and/or electrochemical stability limits of electrocatalysts [26–28]. It can also be used to numerically evaluate and compare the stability of different catalysts (S-number [29], activity-stability factor [30]).

Originally developed in 2000 by Ogle and Weber for the detection of anodic dissolution of 304 Stainless steel [31], electrochemical flow cell coupled (EFC) with an inductively coupled plasma–optical emission spectroscopy (ICP-OES) device or an ICP-MS is still a young methodology in the field of electrocatalysis.

The widespread use of this methodology for electrocatalysts studies can be attributed to Mayrhofer et al. and their so-called scanning electrochemical flow cell (SFC) (Fig. 1**a**) [22,32], which sparked the utilisation of ICP-MS in the electrocatalysis field. In their setup, the cell is characterised by a small wetted area (2.56×10^{-3} cm^2), a low internal volume (5 µL cell, 21 µL tubing) and a dead time of around 30 s (for a liquid flow of 51 µL/min). It is therefore called a microelectrochemical cell. In addition, their setup is combined with an XYZ-positioning system which allows easy and fast sample exchange. Surprisingly, it was only eight years after the publication of such a setup that Cherevko et al. investigated the impact of the setup geometry on the obtained dissolution results [33]. The authors showed that time resolution is related to the residence time distribution (RTD): the lower the residence time, the better the resolution. However, RTD presents some asymmetry due to mass transport in the outlet capillary. The authors also optimised their cell with an angle $\geq 60°$between the inlet and the outlet channels while the flow rate was set to be between 200 and 300 µL/min.

Another setup was introduced by Markovic's group. Lopes et al. presented a stationary probe rotating disc electrode (SP-RDE) coupled with an ICP-MS (450 µL/min, delay time of ~5.5 s and total internal volume of ~42 µL, Fig. 1**b**) [25]. This setup allows one to control the mass transport properties at the electrode surface. This results in low dissolution rates measured but enables the correlations between the structure and both the activity and stability of electrocatalysts. However, the separation of cathodic-related and anodic-related dissolution processes was not achieved with this setup, and only a relatively noisy signal can be observed.

In our group, we employed a third variation of electrochemical cell coupled with ICP-MS setup for metal dissolution detection, so-called electrochemical flow cell-ICP-MS (EFC-ICP-MS) [14,34,35]. This setup is based on a commercially available BASi-cell design © and thus most of the parts are commercially available (Fig. 1**c**). Consequently, some derivative versions have made it, arguably, the most employed setup in the community [36–40] albeit the setups from other groups are also custom made and thus some differences arise. For example, the cell from Choi et al. has a defined cell volume and their arrangement allows to use a glassy carbon rod of a Pt wire as the counter electrode [36,38]. Similarly, Maillard et al. can also introduce a glassy carbon rod as counter electrode in their homemade PEEK cell [40]. Nonetheless, in all these setups, the cell volume is defined by the PEEK cell, oppositely to the two previously introduced setups (SP-RDE and SFC). In our case, a (silicon) gasket separates the two walls of the cell and defines the internal volume. Moreover, in contrast to SFC and SP-RDE setups, an external pump can be used to control the flow of electrolytes instead of the ICP-MS peristaltic pump (Fig. 1**d**). Furthermore, it can be used with a cross flow switch therefore enabling the easy and quick change of electrolyte during experiments if necessary.

Nonetheless, this is an overall young methodology in the field of electrocatalysis and although various models and setups have been developed, the influence of experimental parameters (apart from the electrochemical protocol itself) on dissolution results has rarely been investigated. Except for the previously mentioned theoretical study by Shkirskiy et al. on SFC-ICP-MS [33], the importance of cell and other

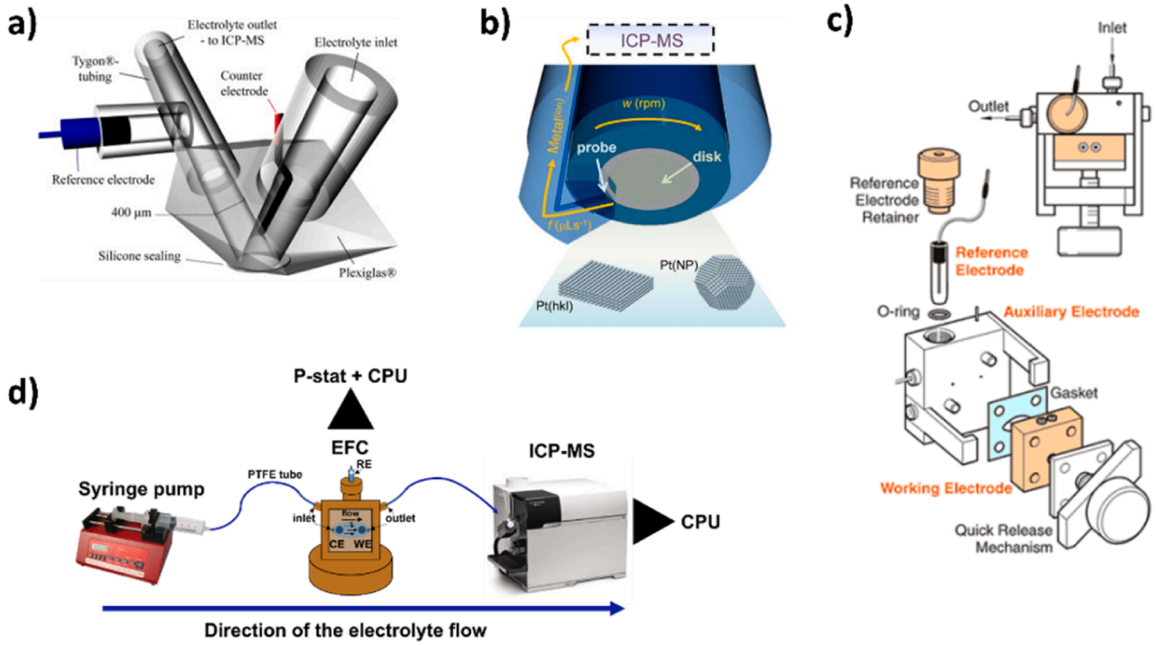

Fig. 1. Different electrochemical cells coupled with an ICP-MS. a) Scanning-flow-cell presented by Mayrhofer et al. Reproduced with permission [22]. Copyright 2011, Elsevier. b) Stationary probe – rotating disk electrode presented by Markovic et al. Reproduced with permission [25]. Copyright 2016, American Chemical Society. c) Scheme of the electrochemical flow cell presented by our group. Reproduced with permission[26]. Copyright 2017, American Chemical Society. d) Scheme of the full EFC-ICP-MS setup.

non-electrochemical experimental parameters have to the best of our knowledge not been studied yet. Furthermore, the intrinsically low concentrations (ppb range or lower) studied with this method could be influenced by the cell design. Indeed, the dissolution of metals in the operational range of fuel cell (FC) is low and can be influenced by redeposition phenomena, problems of signal/noise ratio or overlapping of the peaks. Interpreting extremely low-resolution signals can be challenging, with the possibility of it being impossible. In the best-case scenario, accurate interpretation of the peaks would require a profound background knowledge.

Henceforth, we experimentally investigated the impact of several parameters, such as the cell volume, the electrolyte flow speed and the length of the tubing between the outlet of the EFC and the inlet to the ICP-MS, on the PtCo/C electrocatalyst dissolution profile in acidic electrolyte. The impact on the peak resolution and therefore the separation and recognition of different dissolution phenomena and dissolution mechanisms, as well as the impact on the redeposition of metal, are highlighted. Namely, the separation of dissolution peaks has been improved compared to previously published results [14,18,36,39] and the Pt-redeposition has been to a certain degree hindered, which allows for studies in narrower potential windows and/or faster scan rate, namely accelerated degradation studies. Furthermore, the observed phenomena have been confirmed by simulation. A modelling study of the volumetric flow rate and cell volume confirmed the lower redeposition. Finally, the improved system was employed to study the dissolution at FC load-cycle operation relevant potential window, i.e. from 0.85 V_{RHE} to a varying lower potential limit (0.65 to 0.4; 0.05 step V_{RHE}). We note that under these conditions, the metal dissolution is extremely low, so it has been difficult to measure it under dynamic conditions and still distinguish between cathodic and anodic peaks at this potential window [36]. For instance, in one of the rare examples of prior work, some Pt-dissolution signal was achieved at 0.85 V_{RHE} only with 30min accumulation time [41]. Hereby, we were able to visualise both anodic and cathodic dissolution peaks at the FC narrow operational potential window already at room temperature. The comparison of the two setups for this particular case highlights the benefits of the new system as new knowledge can be acquired.

2. Experimental

2.1. Synthesis of the experimental Pt-Co/C

The experimental Pt-Co/C electrocatalyst produced by ReCatalyst d.o.o. (Slovenia) was prepared in accordance with the processes already reported previously [42–44]. Briefly, the experimental electrocatalyst has been prepared in three steps. In the first step, Pt NPs were deposited onto a commercial carbon black support (Ketjen Black EC300J, Impag Group, Switzerland) via the double passivation galvanic displacement method. In the second step, the prepared composites with deposited Pt NPs were thermally annealed in order to obtain the Pt-Co alloy. In the last step de-alloying (acid washing) was performed to de-alloy the catalyst and obtain a Pt-rich overlayer over a Pt-Co core.

2.2. Electrochemical flow cell ICP-MS

The catalysts dissolution was studied in an electrochemical flow cell coupled to an inductively coupled plasma mass spectrometry (EFC-ICP-MS, Fig. 1**d**). The ICP-MS (Agilent 7900, Agilent Technologies, USA) is equipped with a MicroMist glass concentric nebuliser, and a Peltier cooled Scott-type double pass quartz spray chamber. The ICP-MS parameters were kept constant while the cell was modified as described in the results and discussion section. The electrochemical cell is custom-made from PEEK material, based on a commercial cell design (BASi). The working and counter electrodes (WE and CE, respectively) are glassy carbon discs while an Ag/AgCl electrode was used as reference electrode (RE). Its potential against Reversible Hydrogen Electrode (RHE) was evaluated prior to the experiment against a hydrogen reference electrode. PtCo thin films were prepared by drop-casting 5 µL of a 1 mg/mL ink, prepared with Milli-Q water. The ink was sonicated preceding the drop-casting to ensure homogeneity. Afterwards, a drop (5 µL) of a Nafion:Isopropanol (1:50) solution was drop casted to cover both the WE and the CE to ensure the films stability. Several films were prepared and only the best, most homogeneous, films were chosen for experiments. The experiments were performed on several films to ensure reproducibility.

Tubing (diameter of 0.18 mm, PEEK) of different lengths were employed to examine the impact of delay time between the EFC and the ICP-MS. This leads to two different setups, long (L, ~ 50 cm) and short (S, ~ 6.5 cm) systems, implying difference in the delay time between the electrochemical process in the cell and the signal response in ICP-MS. On the other hand, as the gasket defines the cell volume, several thicknesses (two of them are highlighted in this work – high internal volume (HIV) and low internal volume (LIV)) were investigated (**Figure S2**). Finally, the flow of the electrolyte was varied for different experiments (400 µL/min and 600 µL/min) but kept constant during the time of one experiment. It was controlled by a mechanical syringe pump (AL-1000, World Precision Instrument, USA). The different setups are summarised in Table 1.

2.3. Electrochemical protocols

The electrochemical protocols were controlled by an Ivium potentiostat (Ivium Technologies, Netherlands). Two sets of experiments were performed. First, the impact of experimental parameters was studied by cycling a homemade Pt-Co catalyst between 0.05 and 1.2 V_{RHE} at different scan rates (10, 20, 50, 100, 200, 300, 500 mV/s). The system was free to be at OCP for two minutes between each set of 5 cycles at different scan rate.

Afterwards, the impact of the potential window on Pt-Co dissolution was studied in both the old setup (L-HIV-cell) and the improved setup (S-LIV-cell). Namely, three cycles between 0.85 V_{RHE} and a varying lower potential limit (0.7 to 0.4; 0.05 step V_{RHE}) were performed.

2.4. Profilometry measurement

The film thickness was measured with a Profilometer (Z-gage, Zygo Ametek, USA). The cell used in the electrochemical flow cell was directly put under the device and the thickness of the film was measured two times, before and after adding the ionomer (Nafion).

2.5. Flow-cell model

A three-dimensional model was employed to imitate the cell. It consisted of an oval domain representing the internal space of the cell, two circular boundaries representing the WE and CE, and two short tubes for the inlet and outlet. The parameters of the model cell are summarised in **Table S1** and the cell geometry is shown in Fig. 2. For better visibility of the cell, the tubing within the model has been shown shorter than in the real experiment. Dynamic continuum mechanics modelling was employed to simulate the cell behaviour. Further explanation of the model construction can be found in supplementary information.

Table 1
Different EFC-ICP-MS setups.

	Long tubing	Short tubing
High Internal Volume	L-HIV-cell	S-HIV-cell
Low Internal Volume	L-LIV-cell	S-LIV-cell

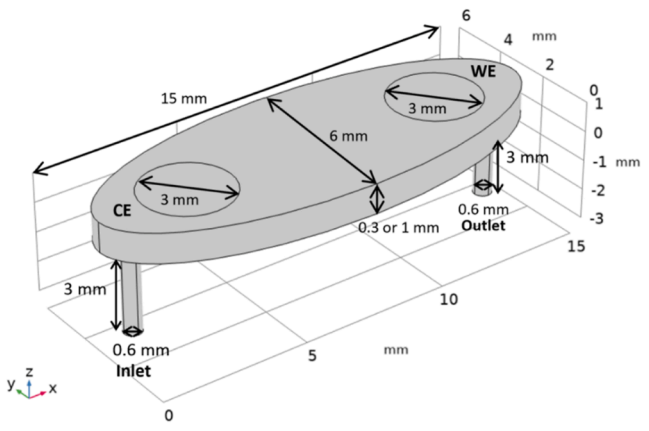

Fig. 2. Cell geometry used for the model construction.

3. Results and discussion

In order to test the impact of the experimental parameters on the dissolution results, the electrochemical protocol was kept constant while the EFC-ICP-MS setup was modified. Namely, the experimental ReCatalyst Pt-Co electrocatalyst was cycled between 0.05 and 1.2 V_{RHE} at different scan rates. Five cycles have been performed for each scan rate and the system was left at OCP for 120 s in between each scan rate (see **Figure S3** for protocol).

The first section of the EFC-ICP-MS setup that has been modified was the length of the outlet tubing that connects the EFC with the ICP-MS. This has been done to shorten the dead time for dissolved metals in the EFC to reach the nebuliser of the ICP. A flow of 400 μL/min was kept constant for this round of experiments. Dead time of < 5 s has been measured in the short tubing-setup (S-cell, length $\sim$ 6.5 cm, diameter 0.18 mm) compared to 25–28 s for the long tubing-setup (L-cell, length $\sim$ 50 cm, diameter 0.18 mm). Consequently, the diffusion of dissolved species is limited, and sharper peaks are observed (Fig. 3 and **Figure S4** for the full protocol) [18]. As shown in the case of a scan rate of 10 mV/s (Figs. 3**a** and 3**c**), the use of S-cell in contrast to the use of the L-cell enables a clear separation of both the anodic (Peak 2 for Co) as well as cathodic (Peak 3 for Co) dissolution peaks. In contrast, for the L-cell the cathodic dissolution Co peaks (3) are only visible as the tail/shoulder peaks to the more intense anodic dissolution Co peaks (2). Also, in the case of Pt-dissolution, clear separation of the anodic (2′) and cathodic (3′) dissolution peaks is visible for the S-cell, whereas the resolution of both Pt-dissolution peaks has been visibly impacted in the case of the L-cell. Furthermore, we observe another low intensity Co dissolution peak (1), which has in the case of the L-cell been only observed as an extension of the tail/shoulder dissolution peak, facilitating the interpretation of results. In this case, three peaks can be observed in the dissolution profile of Co during slow cycle (Fig. 3**a**), especially for the S-cell. The mechanistic nature behind all the mentioned dissolution peaks has been already well reported in our prior work [14,18,43,45,46]. Briefly, the first peak (1) is attributed to the Co underpotential/overpotential deposition. This peak has previously been already observed for various transition metals (Cu, Ni, Fe, Co) [14,18]. It should be noted that one could expect a lower baseline in the potential window of metal deposition. Indeed, the less noble metal can redeposit on the catalyst and thus a drop in dissolution can be observed as seen by Roiron et al. for PtNi [40]. However, significant redeposition should take place compared to the constant dissolution (background) to directly observe the decrease in dissolution. In our system, a tail of dissolution from the previous cathodic peak is visible at the moment of under potential deposition which would make this observation more difficult. Afterwards, the previously deposited Co is available for dissolution in the following cycles where the peak 1 is observed. On the other hand, the other peaks are a consequence of well-reported transient dissolution of metal. Namely, metals are known to dissolve during the oxidation process (peak 2, anodic dissolution) as well as during the reduction process (peak 3, cathodic dissolution), whereas we are able to correlate peaks 2 and 3 corresponding to the Co anodic and cathodic dissolution as a direct consequence of the Pt anodic and Pt cathodic peaks 2′ and 3′. Despite a two times faster scan rate (10 mV/s) in comparison to our prior

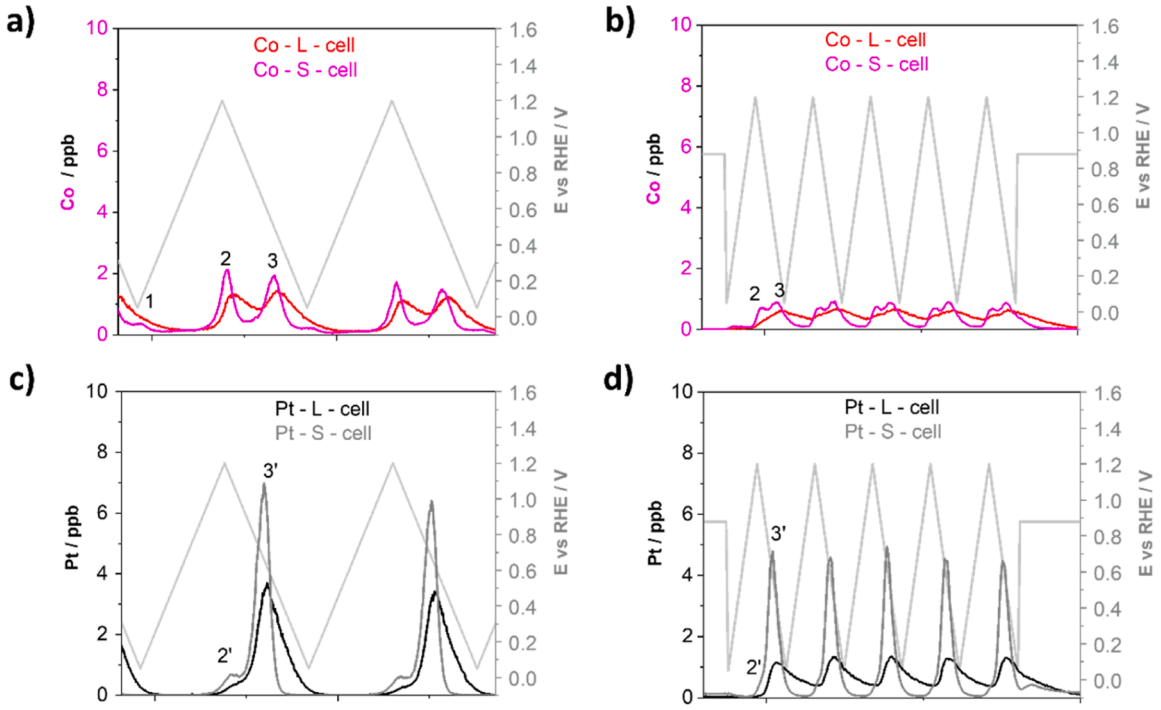

Fig. 3. Comparison of the dissolution profile of Pt (black) and Co (red) in two setups with different outlet tubing lengths; L-cell and S-cell. a) During 2 cycles between 0.05 and 1.2 V_{RHE} at 10 mV/s (cycles number 2 and 3 are shown). b) During 5 cycles between 0.05 and 1.2 V_{RHE} at 50 mV/s.

reported research [18] the dissolution peaks remain well-resolved at a higher scan rate in the S-cell, thus allowing for faster dissolution data acquisition, and/or evaluations of prolonged experimental protocols, i.e. accelerated degradation tests (ADT). The improvement in resolution becomes even more significant if we further increase the scan rate to 50 mV/s (Figs. 3**b** and 3**d**). In this case, we still notice a separation of the peaks 2 and 3 corresponding to Co dissolution for the S-cell, whereas only a single broad peak is observed in the case of the L-cell. The exact same trend is also observed in the case of Pt-dissolution (peaks 2′ and 3′).

Finally, the dissolution signal has also been integrated (Table 2) in order to obtain the total dissolution of Pt and Co during two slow cycles (Figs. 3**a** and 3**c**; 10 mV/s, cycles 2 and 3) as well as five faster cycles (Figs. 3**b** and 3**d**; 50 mV/s). The cycles 2 and 3 were integrated in the case of slow cycling. The cycle 1 was not integrated on purpose to avoid any interference due to a possible dissolution induced by the jump from OCP to the starting potential. And thus, possible error in assessing the intrinsic dissolution during electrochemical cycling. The graph's zero was used as a baseline for the integration. It can be observed that the total integrated quantities of Pt and Co dissolutions are within the margin of error. However, what can be observed is that the error of acquiring dissolution data from multiple measurements using the S-cell is lower for both the Pt and Co dissolution in the case of both evaluated scan speeds. On the other hand, the explanation of why the dissolution is decreasing with a higher scan rate has already been reported [47]. Namely, a lower (slower) scan rate results in an overall longer exposure of the Pt-based nanoparticles at both oxidising (during anodic scan) and also reducing (during cathodic scan) potentials. Consequently, more Pt-oxide is accumulated during the anodic scan, followed by also reduction of more Pt-oxide during the cathodic scan and thus, more transiently dissolved Pt, which is in the case of Pt-alloys also followed by the dissolution of the transition metal (in this case Co).

As limiting the diffusion of dissolved species seemed efficient to improve the peak resolution, a faster electrolyte flow (600 μL/min vs 400 μL/min) has also been investigated (Fig. 4, full protocol in **Figure S5**) in addition to the use of a shorter setup (S-cell). Surprisingly, the faster flow actually resulted in a measurement of a decreased amount of metal dissolution for both Co as well as Pt with a very insignificant additional benefit in the improvement of the peak resolution. In this case, the flow has to be taken into account while calculating the metals dissolved amount during cycling, and thus the dissolved mass is presented in Table 3 instead of a concentration, this is not necessary if the flow is kept constant between experiments (other cases). In the case of 600 μL/min electrolyte flow rate, the Pt dissolution decreased by almost a factor of two in contrast to the electrolyte flow rate of 400 μL/min for fast scan rate cycles (50 mV/s) while the decreased is lower for the slow cycles, i.e. Pt dissolution at 600 μL/min is around 80 % of the dissolution at 400 μL/min (Table 3). No difference was noticeable for Co dissolution, but still noticeable at slower scan rates (10 mV/s). This result indicates that changing parameters to reduce the redeposition of Pt is not as straight forward as it seems. One part of the explanation most likely originates from the limitation of the nebuliser capability in the ICP-MS, which is not optimised for flows as high as 600 μL/min and thus, also leads to less dissolved species being transported to the MS detector. However, the observed lower dissolution cannot solely be ascribed to that phenomenon as the calibration was performed under the same conditions. Most likely, the higher flow is also inducing a turbulent behaviour inside the cell and thus enables more Pt to redeposit and thus also blocks Co dissolution. More precisely, a laminar flow would directly bring any dissolved species to the ICP-MS while a turbulent behaviour would allow the species to reach the electrodes again after their dissolution and thus higher redeposition would take place if the flow is too high.

Another approach that has been investigated in order to increase the resolution of the metal dissolution peaks has been to vary (decrease) the flow-cell volume. In our setup, this can be achieved by changing the gasket thickness. The volume inside the flow cell is decreased by using a

Table 2
Dissolution of Pt and Co in two different setups and during different protocols. The errors are based on 3 measurements under the conditions reported in Fig. 3. The cycles number 2 and 3 were integrated in the case of slow cycling.

	Pt dissolution for 2 slow cycles (ppb)	Co dissolution for 2 slow cycles (ppb)	Pt dissolution for 5 fast cycles + OCP (ppb)	Co dissolution for 5 fast cycles + OCP (ppb)
L-cell	422 ± 111	230 ± 46	205 ± 30	99 ± 19
S-cell	343 ± 45	233 ± 31	257 ± 41	107 ± 10

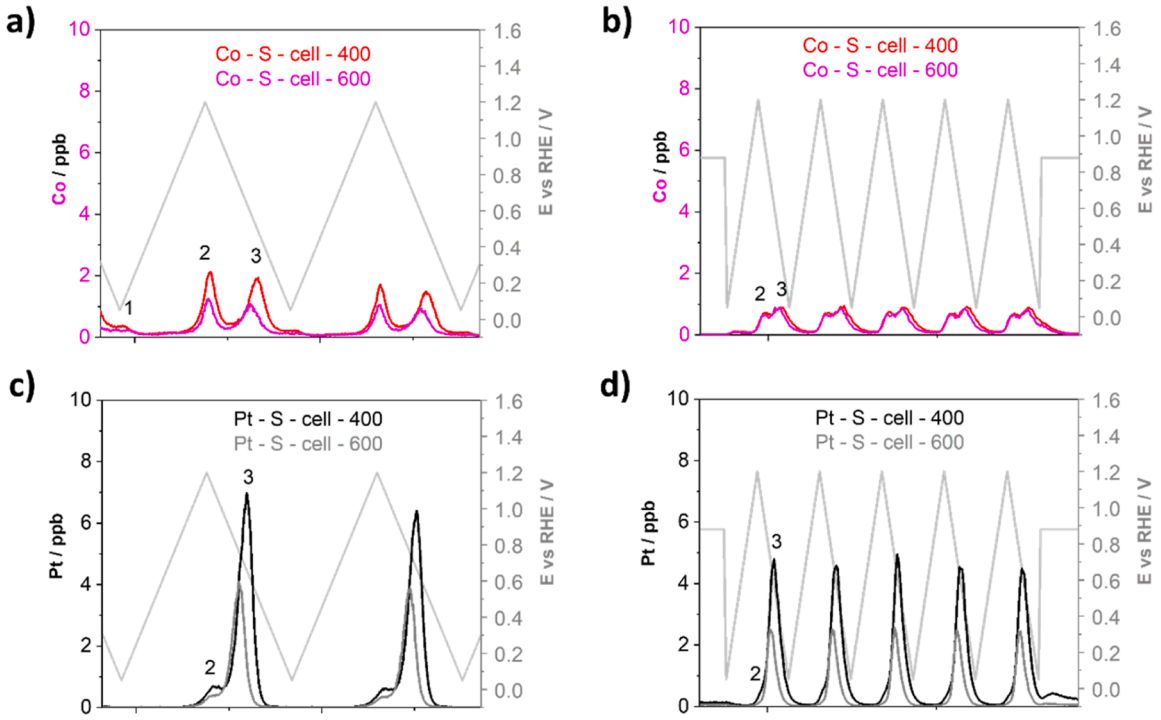

Fig. 4. Comparison of the dissolution profile of Pt (black) and Co (red) in the S-cell with two different flow rates; 400 µL/min and 600 µL/min. a) During 2 cycles between 0.05 and 1.2 V_{RHE} at 10 mV/s (cycles number 2 and 3 are shown). b) During 5 cycles between 0.05 and 1.2 V_{RHE} at 50 mV/s.

Table 3
Dissolution of Pt and Co in S-cell with different flow rates. The errors are based on 3 measurements under the conditions reported in Figure 3. The cycles number 2 and 3 were integrated in the case of slow cycling.

	Pt dissolution for 2 slow cycles (ng)	Co dissolution for 2 slow cycles (ng)	Pt dissolution for 5 fast cycles + OCP (ng)	Co dissolution for 5 fast cycles + OCP (ng)
400 µL/min	2.3 ± 0.17	1.56 ± 0.11	1.72 ± 0.13	0.7 ± 0.05
600 µL/min	1.89 ± 0.14	1.42 ± 0.11	1.08 ± 0.08	0.92 ± 0.07

thinner gasket, which under a constant electrolyte flow means that the electrolyte is being replaced more rapidly and thus, there is less probability for any redeposition of the dissolved species in the cell. Prior to the metal dissolution evaluation, the film thickness was measured with a profilometer (**Figure S6** without Nafion and **Figure S7** with Nafion) to ensure that the decrease of the gasket thickness does not lead to a potential contact between the electrocatalyst film and the gasket. Additionally, one should also keep in mind that lowering the internal volume of the cell while keeping the same flow rate of electrolyte is still increasing the shear forces imposed on the electrocatalyst film. Therefore, if the volume is decreased too dramatically, one could lose the film integrity (in other words parts of the electrocatalyst thin film falling off), leading to false dissolution results. Finally, using too thin gaskets can also result in leakage of electrolyte due to insufficient sealing – this could, in theory, be improved by a higher precision and lower tolerances of EFC manufacturing, allowing for less margin of gaps that need to be filled by the thickness of the gaskets to allow for adequate sealing and prevention of the electrolyte leakage.

For the metal dissolution data acquisition, two different gaskets of different thicknesses have been investigated. The commercial BASi gasket was 1 mm thick, resulting in an internal cell volume of 47.12 µL. For thinner gaskets, a modified 0.3 mm silicon-based gasket has been employed with an internal cell volume of 14.14 µL (~2/3 decrease of the internal volume). In addition, the impact of the gasket thickness has been investigated with both the S-cell as well as L-cell. In both cases, the thickness of the gasket (and thus the internal volume of the cell) seems to have an insignificant impact on the transition metal dissolution (Co) while impacting greatly the Pt dissolution (Fig. 5, full protocol in **Figure S8**). Namely, once again the total dissolution of the metal was calculated for two cycles at 10 mV/s and for 5 cycles at 50 mV/s and compared between the different setups (Table 4). As previously discussed (see discussion related to Table 2), the length of the tubing does not affect the dissolution amount (422 ± 111 ppb for L-HIV-cell vs 343 ± 45 ppb for S-HIV-cell) but leads to sharpest peaks. On the other hand, the internal volume of the cell impacts the amount of dissolved species reaching the detector, most likely by limiting the redeposition. Indeed, the dissolution of Pt is around two times higher with the LIV-cell (905 ± 107 ppb for S-cell and 848 ± 9 ppb for L-cell) than with the HIV-cell (343 ± 45 and 422 ± 111 ppb for S-cell and L-cell, respectively) for two slow cycles. On the contrary, the dissolution of Co is relatively similar in all the setups (Table 4). This hints at the decrease in Pt redeposition as hypothesised in a previous study, whereas the transition metal is typically not affected by this phenomenon [43]. Therefore, one should keep in mind that the assessed dissolution, and consequent stability, can be underestimated or overestimated while using online-ICP-MS studies, if one does not, for instance, also consider the impacts of the measurement conditions on the redeposition of Pt. This also includes our previously studied effect of temperature on the metal dissolution where a higher electrolyte temperature has been shown to result in an increased redeposition of Pt as well [44]. Nevertheless, the comparison of various electrocatalysts within the same EFC-ICP-MS setup using the same measurement conditions will still provide for highly valuable stability

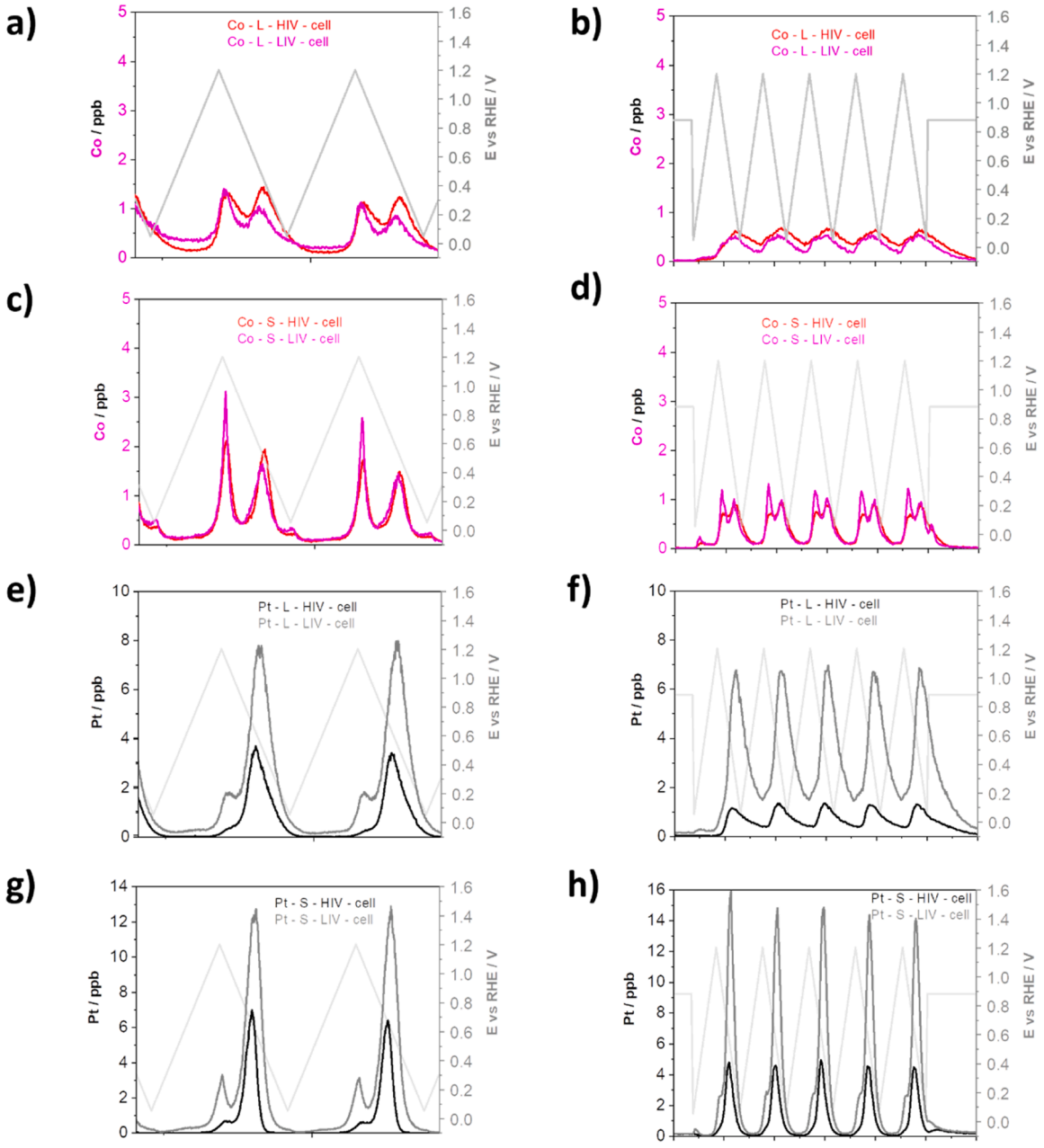

Fig. 5. Comparison of the dissolution profile of Pt (black) and Co (red) while modifying the internal volume of the cell. The comparison was performed on both L-cell (a, b, e and f) and S-cell (c, d, g and h). a) and c) During 2 cycles between 0.05 and 1.2 V_{RHE} at 10 mV/s (cycles number 2 and 3 are shown). b) and d) During 5 cycles between 0.05 and 1.2 V_{RHE} at 50 mV/s.

Table 4
Dissolution of Pt and Co in two different setups and during different protocols. The errors are based on 3 measurements under the conditions reported in Figure 4. The cycles number 2 and 3 were integrated in the case of slow cycling.

	Pt dissolution for 2 slow cycles (ppb)	Co dissolution for 2 slow cycles (ppb)	Pt dissolution for 5 fast cycles + OCP (ppb)	Co dissolution for 5 fast cycles + OCP (ppb)
L-HIV-cell	422 ± 111	230 ± 46	205 ± 30	99 ± 19
L-LIV-cell	848 ± 9	223 ± 26	707 ± 114	87 ± 1
S-HIV-cell	343 ± 45	234 ± 31	257 ± 41	107 ± 10
S-LIV-cell	905 ± 107	227 ± 19	680.8 ± 120	102 ± 9

trends. Additionally, the lower internal volume and subsequent lower redeposition leads to sharper peaks, especially for Pt and at a high scan rate. Indeed, the Pt anodic dissolution peak (labelled by 2 in Fig. 3) becomes more visible while using a lower internal volume for the cell (Fig. 5**e** and 5**g**). Although the effect is observable in both cases, it is more observable in the S-cell than L-cell. However, it is difficult to

quantify the improvement in resolution for this peak as it is not properly resolved in both L-cells as well as in the S-HIV-cell. The width at half maximum of the peak cannot be accurately determined due to the high baseline. Similar effect is observed for Co with a clearer separation between the anodic and cathodic peaks in the case of S-cell, particularly at a higher scan rate (Fig. 5**a–d**). This highlights the importance of low cell volume to limit the redeposition.

In order to understand these behaviours, 3D modelling of the cell has been performed where the flow velocity inside, and the Pt ions concentration at the working electrode were calculated. Firstly, the hydrodynamic behaviour of the cell has been studied, in particular, the volumetric flow rate and cell volume were varied. The model

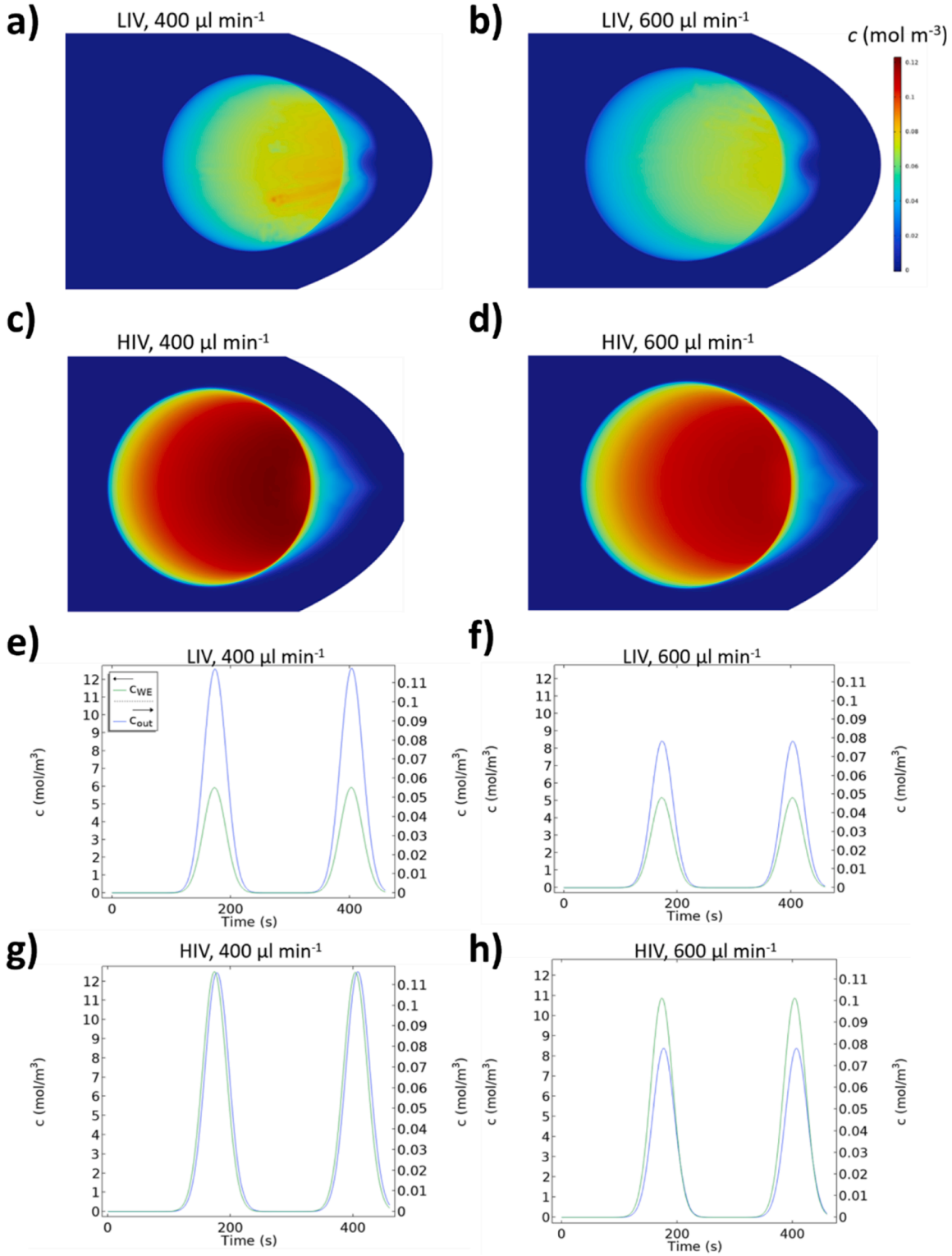

Fig. 6. Pt ions concentration at the WE surface and its close vicinity at the time of 115 s (corresponding to 1.2 V, the highest value of potential in the experiments) (a-d). Evolution of concentrations at the WE (c_{WE}, green curve, left y-axis) and at the outlet (c_{out}, blue curve, right y-axis) in time for the two cell geometries and two flow rates (e-h).

(**Figure S9**) confirms that velocity rises with increasing flow rate and decreasing thickness.

Pt concentration on the WE surface and its vicinity is shown in Fig. 6**a–d** and it follows a similar trend as the velocities shown in **Figure S9**. In particular, the concentrations are lower in the LIV cells due to higher local velocities inside the cell. Similarly, a higher flow rate also results in a lower surface concentration. It is worth emphasising here that the Pt dissolution rate was considered the same in all studied cases, although it is known that the concentration of dissolved species in the electrolyte has a direct effect on its dissolution rate (or equilibrium potential) via the thermodynamic relationship described by the Nernst shift [48]. In principle, a higher concentration of Pt ions in the electrolyte will slow down Pt dissolution from the catalyst and at the same time also cause more Pt to redeposit [49]. Thus, catalyst will seem more stable.

In Fig. 6**e–h**, time evolutions of average WE surface concentrations and outlet concentrations are plotted. The graph shows that the outlet concentrations change notably with the variation of flow rate and only slightly depend on the cell thickness. As for the WE, higher cell volume and lower flow rate result in higher surface concentrations. Therefore, it seems that the difference of measured Pt ions with various flow rate (Fig. 4) is mostly attributed to the difference in Pt ions amount reaching the EFC outlet, namely some Pt stays in the cell and redeposits. On the other hand, the difference in internal volume clearly leads to a difference in concentration on the WE at both the maximum potential (Fig. 6, at 1.2 V_{RHE}) and lower potential (**Figure S10**, at 0.05 V_{RHE}). Consequently, a higher amount of Pt ions is available for higher volume as well as lower flow to redeposit on the WE electrode instead of reaching the outlet of the cell and the ICP-MS detector.

Additionally, Fig. 7 shows how the flow affects the space distribution of concentration in a vertical plane in the middle of the cell. The concentrations in the LIV-cell are distributed in a ribbon-like manner, and the ions flow directly to the outlet channel, whereas the HIV-cell concentrations are more spread out and reach the parts right of the outlet. Similarly, the distribution of the streamlines of the flow supports the concentration distribution related to the different cell thicknesses (**Figure S11**).

Afterwards, the values of c_{final} are compared to the experimental results. Table 5 shows the values of c_{final} calculated for the two geometries and two flow rates. Regarding the effect of the electrolyte flow rate, the resulting model ratio $\frac{c_{final}(600\ \mu l\ min^{-1})}{c_{final}(400\ \mu l\ min^{-1})} = 0.67$ regardless of the cell thickness. However, Table 3 shows the experimental results for the two flow rates, providing a notably different ratio of $\frac{c_{final}(600\ \mu l\ min^{-1})}{c_{final}(400\ \mu l\ min^{-1})} = 0.82$. This suggests lower amount of dissolved Pt during the experiments with a higher flow rate. Presumably, higher velocity along the WE surface would lead to faster transport of dissolved Pt from the electrode, resulting in lower surface concentrations, and thus lower inhibition of Pt dissolution or further lower redeposition. Consequently, the ratio would be higher. However, a purely hydrodynamic model cannot explain this behaviour fully, and the kinetics of Pt dissolution and redeposition and the limits of detection by ICP-MS also play a role.

Table 5
Final integrated Pt concentration from the model for the two cell volumes and two volumetric flow rates, calculation described in the Supplementary Information (Equation S6).

Cell and flow rate	C_{final} (ppb)	C_{final} (10^{-2} mol/m^3)
LIV 400	439	2.43
LIV 600	293	1.62
HIV 400	439	2.43
HIV 600	293	1.62

As for the effect of different cell volumes, Table 4 shows the respective experimental results, and for the two-cycle experiments, the HIV outlet concentrations are less than half of the corresponding LIV ones. The model results in Table 5 show that it was not caused by the hydrodynamics of the flow and hypothetical Pt ion accumulation in the cell. A plausible explanation lies, again, in the effect of Pt concentration at the WE surface on the kinetics of Pt dissolution and redeposition. Furthermore, the experimental results agree well with the WE surface concentrations in Fig. 6**a–d** where thinner cells exhibited lower values.

As the last step, we have decided to combine the lessons learned and demonstrate the added value of the improved system (short setup with a thinner gasket) by evaluating the metal dissolution of the experimental Pt-Co electrocatalyst under potential windows that are more relevant to the FC operation. Namely, this included cycling of the evaluated electrocatalyst between 0.85 V_{RHE} and a lower potential that was varied from 0.7 to 0.4 V_{RHE}. Dissolution data at such voltage windows is of

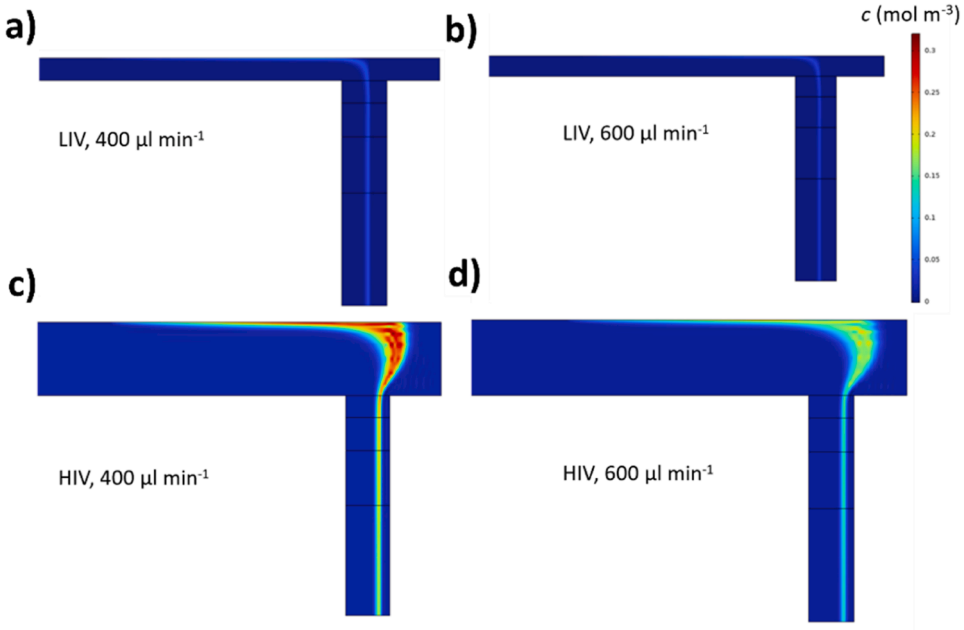

Fig. 7. Pt ion concentrations field along the vertical middle plane across the cell. a) In LIV-cell at 400 µL/min. b) In LIV-cell at 600 µL/min. c) In HIV-cell at 400 µL/min. d) In HIV-cell at 600 µL/min.

particular importance in understanding the degradation mechanisms of Pt-based electrocatalysts that correspond more closely to the FC stack operating conditions. Fig. 8 shows the comparison of Pt and Co dissolution in the two different setups (both ends of the 'extreme'), i.e. L-HIV-cell and S-LIV-cell. In the case of the experiment with L-HIV-cell, only one peak of dissolution was observed for both Pt and Co (Fig. 8**a**) albeit at a lower potential limit a shoulder becomes visible in the Co dissolution profile. The observed peak (1) is related to the cathodic dissolution process with the Pt going away and followed by the unprotected Co dissolving as a consequence (1′). Similarly to the dissolution mechanism observed while cycling in a wider potential window (Fig. 2), the second peak/shoulder in Co dissolution (2′) is attributed to oxidation-related dissolution. In the wide potential window experiment, a Pt dissolution peak was visible in both setups which then induced the Co dissolution. On the other hand, the FC relevant experiment presents only a transition metal dissolution shoulder for the anodic part of the scan. This peak has been previously reported for Ni and Cu [14]. On the other hand, the S-LIV-cell allows us to detect the Pt anodic dissolution peak for the first time for such narrow potential windows (peak 2 in Fig. 8**b**). Nevertheless, the dissolution amounts in the two setups are fairly similar (Table 6). The signal integration for six cycles was performed on the three cycles between 0.85 and 0.65 V_{RHE} as well as the three cycles between 0.85 and 0.6 V_{RHE}. It is observed that the dissolution recorded in this potential window is similar for both metals in the two setups. However, the signal for the full protocol results in more Pt dissolution in the S-LIV-cell. This is in accordance with the previous results (Figs. 2–4) that suggested that the redeposition of Pt is hindered significantly in the S-LIV-cell. Fortunately, it also means that cycling in the FC range leads to trustable results as long as the range does not reach the Pt deposition potential. Therefore, more distinct separation of peaks was observed with the S-LIV-cell, even at FC operational potential window. The improved dissolution signal allows for a better understanding of the dissolution processes in FC device, with both anodic and cathodic peaks revealed.

4. Conclusion

In conclusion, we have showcased that optimisation of the EFC-ICP-MS setup leads to improved results by limiting the redeposition of Pt ionic species and diffusion of dissolved metal species. Firstly, the dead time was reduced by decreasing the tubing length between the outlet of the EFC and the inlet of the ICP, which provided better-resolved peaks. Notably, the separation between the anodic and the cathodic dissolution peaks has been improved, leading to an easier interpretation of the dissolution mechanism, even at higher scan rates. Additionally, peaks that previously appeared as shoulder using the L-cell are now distinctly visible with the S-cell. Furthermore, it has been confirmed that the two dissolution processes are occurring even at the narrow FC operational potential window. On the other hand, a lower internal volume of the cell limits the redeposition of Pt while not affecting the Co signal. Namely, the recorded Pt dissolution has been improved by a factor of 2.5. The difference in Pt ions concentration at the working electrode as well as the flow rate impact on the hydrodynamic flow were also studied by dynamic continuum mechanics modelling to confirm that the observed dissolution differences between setups were due to the redeposition of Pt. Overall, the optimised setup (short tubing low internal volume cell – S-LIV-cell) can now better resolve the dissolution mechanisms and can also be used to reliably compare different catalysts; however, one must do it with the same setup or in narrow potential windows where little redeposition is taking place. Nonetheless, it has been found that modifying the flow of the electrolyte, which should result in a lower redeposition and potentially higher resolution, led to a lower signal in the ICP-MS. Overall, the highlights of this study can be resumed as:

- A better resolution can be achieved in the ICP-MS signal by shortening the tubing and thus the dead time between the cell and the ICP-MS, which limits the diffusion.
- Lowering the internal volume of the cell hinders the redeposition of metal and thus an increased signal can be obtained.
- Consequently, the dissolution of metals in every EFC-ICP-MS is most likely underestimated compared to RDE (but overestimated compared to real devices [45]).

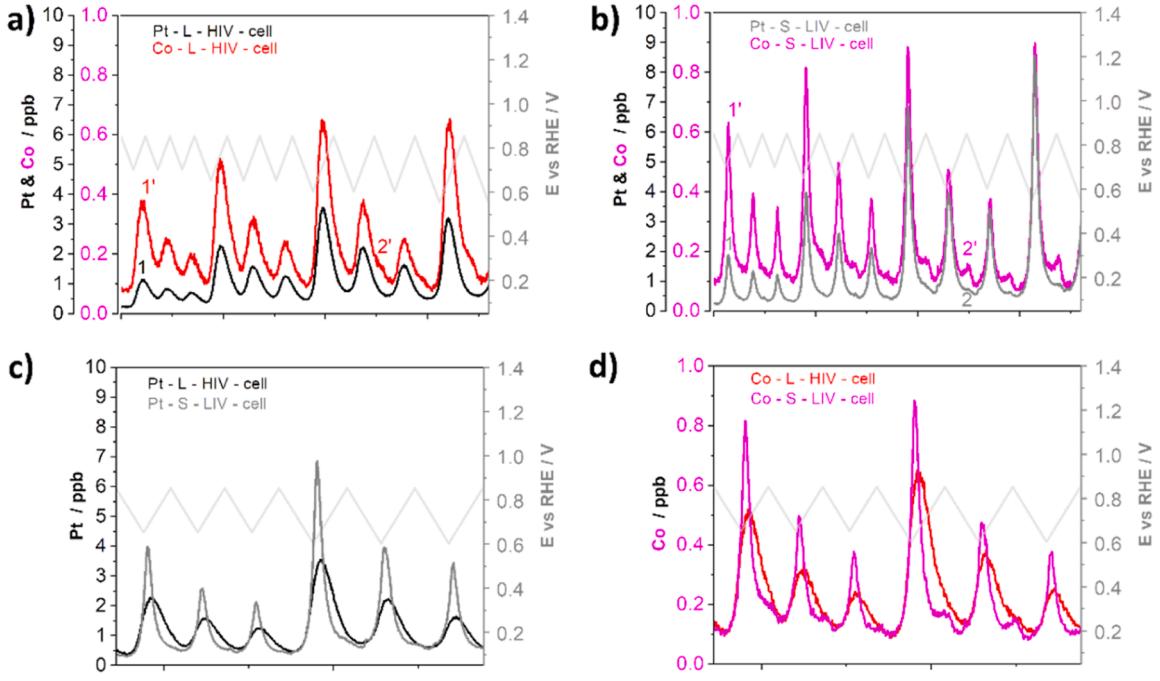

Fig. 8. Comparison of the dissolution profile of Pt (black) and Co (red) during cycles in potential window relevant for real devices. a) Dissolution in the standard setup (L-HIV-cell). b) Dissolution in the optimized setup (S-LIV-cell). c) Comparison of Pt dissolution. d) Comparison of Co dissolution.

Table 6
Dissolution of Pt and Co in the operation range of FCs. Comparison between the two setups. The errors are based on 3 measurements under the conditions reported in Figure 8.

	Pt dissolution for 6 cycles (ppb)	Co dissolution for 6 cycles (ppb)	Pt dissolution all protocol (ppb)	Co dissolution all protocol (ppb)
L-HIV-cell	648 ± 86	125 ± 17	1532 ± 197	352 ± 45
S-LIV-cell	665 ± 88	115 ± 15	2221 ± 285	348 ± 45

- New or more precise mechanisms can be revealed with an optimised setup.
- Less aggressive conditions and/or faster cycles can be performed with acceptable resolution of the dissolution peaks. Anodic and cathodic dissolution are also visible at narrower potential windows.

CRediT authorship contribution statement

Leonard Moriau: Investigation, Methodology, Writing – original draft. **Tina Đukić:** Investigation, Writing – review & editing. **Vojtech Domin:** Software, Writing – original draft. **Roman Kodym:** Software, Writing – review & editing. **Martin Prokop:** Validation, Funding acquisition, Writing – review & editing. **Karel Bouzek:** Funding acquisition, Writing – review & editing. **Matija Gatalo:** Conceptualization, Methodology, Writing – review & editing. **Martin Šala:** Validation, Conceptualization, Writing – review & editing. **Nejc Hodnik:** Funding acquisition, Writing – review & editing.

Declaration of competing interest

The authors declare no competing financial interests. The present manuscript has not been considered for publication elsewhere.

Data availability

Data will be made available on request.

Acknowledgements

The authors would like to acknowledge the Slovenian Research and Innovation Agency (ARIS) programs P2–0393, P1–0034 and I0–0003; the projects N2–0155, N2–0248, N2–0257, J7–4637 and J7–4638; EIC Transition project ENABLER (Grant agreement ID: 101112991); European Research Council (ERC) Starting Grant 123STABLE (Grant agreement ID: 852208) and Proof of Concept Grant StableCat (Grant agreement ID: 966654). The study was also funded by the Czech Science Foundation (GAČR), project No. 22–23668 K. This work was supported by the project "The Energy Conversion and Storage", funded as project No. CZ.02.01.01/00/22_008/0004617 by Programme Johannes Amos Commenius, call Excellent Research.

Supplementary materials

Supplementary material associated with this article can be found, in the online version, at doi:10.1016/j.electacta.2024.144200.

References

[1] I. Katsounaros, S. Cherevko, A.R. Zeradjanin, K.J.J. Mayrhofer, Oxygen as a cornerstone for sustainable energy conversion, Angew. Chem. Int. Ed. 53 (2014) 102–121, https://doi.org/10.1002/anie.201306588.
[2] Y. Wang, K.S. Chen, J. Mishler, S.C. Cho, X.C. Adroher, A review of polymer electrolyte membrane fuel cells: technology, applications, and needs on fundamental research, Appl. Energy 88 (2011) 981–1007, https://doi.org/10.1016/j.apenergy.2010.09.030.
[3] J. Stacy, Y.N. Regmi, B. Leonard, M. Fan, The recent progress and future of oxygen reduction reaction catalysis: a review, Renew. Sustain. Energy Rev 69 (2017) 401–414, https://doi.org/10.1016/j.rser.2016.09.135.
[4] K. Kodama, T. Nagai, A. Kuwaki, R. Jinnouchi, Y. Morimoto, Challenges in applying highly active Pt-based nanostructured catalysts for oxygen reduction reactions to fuel cell vehicles, Nat. Nanotechnol. 16 (2021) 140–147, https://doi.org/10.1038/s41565-020-00824-w.
[5] B. James, Fuel cell systems analysis, DOE hydrogen and fuel cells program, in: 2017 Annual Merit Review Proceedings, 2019. Available from: https://www.hydrogen.energy.gov/annual_review17_fuelcells.html.
[6] M. Escudero-Escribano, K.D. Jensen, A.W. Jensen, Recent advances in bimetallic electrocatalysts for oxygen reduction: design principles, structure-function relations and active phase elucidation, Curr. Opin. Electrochem. 8 (2018) 135–146, https://doi.org/10.1016/j.coelec.2018.04.013.
[7] M. Gatalo, L. Moriau, U. Petek, F. Ruiz-Zepeda, M. Šala, M. Grom, T. Galun, P. Jovanovič, A. Pavlišič, M. Bele, N. Hodnik, M. Gaberšček, CO-assisted ex-situ chemical activation of Pt-Cu/C oxygen reduction reaction electrocatalyst, Electrochim. Acta 306 (2019) 377–386, https://doi.org/10.1016/j.electacta.2019.03.153.
[8] Q. Liu, L. Du, G. Fu, Z. Cui, Y. Li, D. Dang, X. Gao, Q. Zheng, J.B. Goodenough, Structurally ordered Fe3Pt nanoparticles on robust nitride support as a high performance catalyst for the oxygen reduction reaction, Adv. Energy Mater. 9 (2019) 1803040, https://doi.org/10.1002/aenm.201803040.
[9] V.R. Stamenković, B.S. Mun, M. Arenz, K.J.J. Mayrhofer, C.A. Lucas, G. Wang, P. N. Ross, N.M. Marković, Trends in electrocatalysis on extended and nanoscale Pt-bimetallic alloy surfaces, Nat. Mater 6 (2007) 241–247, https://doi.org/10.1038/nmat1840.
[10] H. Lohse-Busch, M. Duoba, K. Stutenberg, S. Iliev, M. Kern, Technology Assessment of a Fuel Cell vehicle: 2017 Toyota Mirai, U.S. Department of Energy, Fuel Cell Technologies Office, 2018. https://publications.anl.gov/anlpubs/2018/06/144774.pdf.
[11] T. Toda, H. Igarashi, H. Uchida, M. Watanabe, Enhancement of the electroreduction of oxygen on Pt alloys with Fe, Ni, and Co, J. Electrochem. Soc. 146 (1999) 3750, https://doi.org/10.1149/1.1392544/meta.
[12] J.R. Kitchin, J.K. Nørskov, M.A. Barteau, J.G. Chen, Role of strain and ligan effects in the modification of the electronic and chemical properties of bimetallic surfaces, Phys. Rev. Lett. 93 (2004) 156801, https://doi.org/10.1103/PhysRevLett.93.156801.
[13] P. Strasser, S. Koh, T. Anniyev, J. Greeley, K. More, C. Yu, Z. Liu, S. Kaya, D. Nordlund, H. Ogasawara, M.F. Toney, A. Nilsson, Lattice-strain control of the activity in dealloyed core-shell fuel cell catalysts, Nat. Chem. 2 (2010) 454–460, https://doi.org/10.1038/nchem.623.
[14] L.J. Moriau, A. Hrnjić, A. Pavlišič, A.R. Kamšek, U. Petek, F. Ruiz-Zepeda, M. Šala, L. Pavko, V.S. Šelih, M. Bele, P. Jovanovič, M. Gatalo, N. Hodnik, Resolving the nanoparticles' structure-property relationships at the atomic level: a study of Pt-based electrocatalysts, IScience 24 (2021) 102102, https://doi.org/10.1016/j.isci.2021.102102.
[15] K. Jayasayee, J.A.R.V. Veen, T.G. Manivasagam, S. Celebi, E.J.M. Hensen, F.A. de Bruijn, Oxygen reduction reaction (ORR) activity and durability of carbon supported PtM (Co, Ni, Cu) alloys: influence of particle size and non-noble metals, Appl. Catal. B 111 (2012) 515–526, https://doi.org/10.1016/j.apcatb.2011.11.003.
[16] E. Antolini, J.R.C. Salgado, E.R. Gonzalez, The stability of Pt-M (M= first row transition metal) alloy catalysts and its effect on the activity in low temperature fuel cells: a literature review and tests on a Pt-Co catalyst, J. Power Sources 160 (2006) 957–968, https://doi.org/10.1016/j.jpowsour.2006.03.006.
[17] L. Dubau, M.Lopez Haro, L. Castanheira, J. Durst, M. Chatenet, P. Bayle-Guillemaud, L. Guetaz, N. Caque, E. Rossinot, F. Maillard, Probing the structure, the composition and the ORR activity of Pt3Co/C nanocrystallites during a 3422h PEMFC ageing test, Appl. Catal. B 142-143 (2013) 801–808, https://doi.org/10.1016/j.apcatb.2013.06.011.
[18] M. Gatalo, P. Jovanovič, U. Petek, M. Šala, V.S. Šelih, F. Ruiz-Zepeda, M. Bele, N. Hodnik, M. Gaberšček, Comparison of Pt-Cu/C with benchmark Pt-CO/C: metal dissolution and their surface interactions, ACS Appl. Energy Mater. 2 (2019) 3131–3141, https://doi.org/10.1021/acsaem.8b02142.
[19] J. Braaten, A. Kongkanand, S. Litster, Oxygen transport effects of cobalt cation contamination of ionomer thin films in proton exchange membrane fuel cells, ECS Trans 80 (2017) 283–290, https://doi.org/10.1149/08008.0283ecst.
[20] J. Durst, M. Chatenet, F. Maillard, Impact of metal cations on the electrocatalytic properties of Pt/C nanoparticles at multiple phase interfaces, Phys. Chem. Chem. Phys. 14 (2012) 13000–13009, https://doi.org/10.1039/C2CP42191G.
[21] R. Singh, P.C. Sui, K.H. Wong, E. Kjeang, S. Knights, N. Djilali, Modeling the effect of chemical membrane degradation on PEMFC performance, J. Electrochem. Soc. 165 (2018) F3328–F3336, https://doi.org/10.1149/2.0351806jes.
[22] S.O. Klemm, A.A. Topalov, C.A. Laska, K.J.J. Mayrhofer, Coupling of a high throughput microelectrochemical cell with online multielemental trace analysis by ICP-MS, Electrochem. Commun. 13 (2011) 1533–1535, https://doi.org/10.1016/j.elecom.2011.10.017.
[23] O. Kasian, S. Geiger, K.J.J. Mayrhofer, S. Cherevko, Electrochemical on-line ICP-MS in electrocatalysis research, Chem. Rec. 19 (2019) 2130–2142, https://doi.org/10.1002/tcr.201800162.

[24] P. Jovanovič, U. Petek, N. Hodnik, F. Ruiz-Zepeda, M. Gatalo, M. Šala, V.S. Šelih, T. P. Fellinger, M. Gaberšček, Importance of non-intrinsic platinum dissolution in Pt/C composite fuel cell catalysts, Phys. Chem. Chem. Phys. 19 (2017) 21446–21452, https://doi.org/10.1039/C7CP03192K.
[25] P.P. Lopes, D. Strmcnik, D. Tripkovic, J.G. Connell, V. Stamenkovic, N. M. Markovic, Relationships between atomic level surface structure and stability/activity of platinum surface atoms in aqueous environments, ACS Catal 6 (2016) 2536–2544, https://doi.org/10.1021/acscatal.5b02920.
[26] P. Jovanovič, N. Hodnik, F. Ruiz-Zepeda, I. Arcon, B. Jozinovic, M. Zorko, M. Bele, M. Šala, V.S. Šelih, S. Hočevar, M. Gaberšček, Electrochemical dissolution of iridium and iridium oxide particles in acidic media: transmission electron microscopy, electrochemical flow cell coupled to inductively coupled plasma mass spectrometry, and X-ray absorption spectroscopy study, J. Am. Chem. Soc. 139 (2017) 12837–12846, https://doi.org/10.1021/jacs.7b08071.
[27] A.A. Topalov, I. Katsounaros, M. Auinger, S. Cherevko, J.C. Meier, S.O. Klemm, K. J.J. Mayrhofer, Dissolution of platinum: limits for the deployment of electrochemical energy conversion? Angew. Chem. Int. Ed. 51 (2012) 12613–12615, https://doi.org/10.1002/anie.201207256.
[28] S. Cherevko, A.R. Zeradjanin, A.A. Topalov, N. Kulyk, I. Katsounaros, K.J. J. Mayerhofer, Dissolution of noble metals during oxygen evolution in acidic media, ChemCatChem 6 (2014) 2219–2223, https://doi.org/10.1002/cctc.20140219.
[29] S. Geiger, O. Kasian, M. Ledendecker, E. Pizzutilo, A.M. Mingers, W.T. Fu, O. Diaz-Morales, Z. Li, T. Oellers, L. Fruchter, A. Ludwig, K.J.J. Mayrhofer, M.T.M. Koper, S. Cherevko, The stability number as a metric for electrocatalyst stability benchmarking, Nat. Cat. 1 (2018) 508–515, https://doi.org/10.1038/s41929-018-0085-6.
[30] Y.T. Kim, P.P. Lopes, S.A. Park, A.Y. Lee, J. Lim, H. Lee, S. Back, Y. Jung, N. Danilovic, V. Stamenkovic, J. Erlebacher, J. Snyder, N.M. Markovic, Balancing activity, stability and conductivity of nanoporous core-shell iridium/iridium oxide oxygen evolution catalysts, Nat. Commun. 8 (2017) 1449, https://doi.org/10.1038/s41467-017-01734-7.
[31] K. Ogle, S. Weber, Anodic dissolution of 304 stainless steel using atomic emission spectroelectrochemistry, J. Electrochem. Soc. 147 (2000) 1770, https://doi.org/10.1149/1.1393433.
[32] A.K. Schuppert, A.A. Topalov, I. Katsounaros, S.O. Klemm, K.J.J. Mayrhofer, A scanning flow cell system for fully automated screening of electrocatalyst materials, J. Electrochem. Soc. 159 (2012) F670, https://doi.org/10.1149/2.009211jes.
[33] V. Shkirskiy, F.D. Speck, N. Kulyk, S. Cherevko, On the time resolution of electrochemical scanning flow cell coupled to downstream analysis, J. Electrochem. Soc. 166 (2019) H866–H870, https://doi.org/10.1149/2.1401915jes.
[34] P. Jovanovič, A. Pavlišič, V.S. Šelih, M. Šala, N. Hodnik, M. Bele, S. Hočevar, M. Garberšček, New insight into platinum dissolution form nanoparticulate platinum-based electrocatalyts using highly sensitive in situ concentration measurements, ChemCatChem 6 (2014) 449–453, https://doi.org/10.1002/cctc.201300936.
[35] P. Jovanovič, M. Može, E. Gričar, M. Šala, F. Ruiz-Zepeda, M. Bele, G. Marolt, N. Hodnik, Effect of particle size on the corrosion behaviour of gold in the presence of chloride impurities: an EFC-ICP-MS potentiodynamic study, Coatings 9 (2018) 10. http://doi.org/10.3390/coatings9010010.
[36] J. Yi, W.H. Lee, C.H. Choi, Y. Lee, K.S. Park, B.K. Min, Y.J. Hwang, H.S. Oh, Effect of Pt introduced on Ru-based electrocatalyst for oxygen evolution activity and stability, Electrochem. Commun. 104 (2019) 106469, https://doi.org/10.1016/j.elecom.2019.05.018.
[37] R.K. Ahluwalia, D.D. Papadias, N.N. Kariuki, J.K. Peng, X. Wang, X. Tsai, D. G. Graczyk, D.J. Myers, Potential dependence of Pt and Co dissolution from platinum-cobalt alloy PEFC catalysts using time-resolved measurements, J. Electrochem. Soc. 165 (2018) F3024, https://doi.org/10.1149/2.0031806jes.
[38] W.H. Lee, H.N. Nong, C.H. Choi, K.H. Chae, Y.J. Hwang, B.K. Min, P. Strasser, H. S. Oh, Carbon-supported IrCoOx nanoparticles as an efficient and stable OER electrocatalyst for practicable CO2 electrolysis, Appl. Catal. B 269 (2020) 118820, https://doi.org/10.1016/j.apcatb.2020.118820.
[39] Z. Wang, E. Tada, A. Nishikata, Communication-cathodic platinum dissolution studied using a channel flow double electrode, J. Electrochem. Soc. 163 (2016) 163, https://doi.org/10.1149/2.104160jes. F421.
[40] C. Roiron, V. Martin, k. Kumar, L. Dubau, F. Maillard, Assessing Pt and Ni dissolution mechanism and kinetics of shapr-controlled oxygen reduction nanocatalysts, Electrochim. Acta 477 (2024) 143760, https://doi.org/10.1016/j.electacta.2024.143760.
[41] S. Cherevko, G.P. Keeley, S. Geiger, A.R. Zeradjanin, N. Hodnik, N. Kulyk, K.J. J. Mayrhofer, Dissolution of platinum in the operational range of fuel cells, ChemElectroChem 2 (2015) 1471–1478, https://doi.org/10.1002/celc.201500098.
[42] M. Gatalo, M. Bele, F. Ruiz-Zepeda, E. Šest, M. Šala, A.R. Kamšek, N. Maselj, T. Galun, P. Jovanovič, N. Hodnik, M. Gaberšček, A double-passivation water-based galvanic displacement method for reproducible gram-scale production of high-performance platinum-alloy electrocatalysts, Ang. Int. Ed. Chem. 58 (2019) 13266–13270, https://doi.org/10.1002/anie.201903568.
[43] L. Pavko, M. Gatalo, G. Križan, K. Ehelebe, F. Ruiz-Zepeda, M. Šala, G. Dražič, M. GeuB, P. Kaiser, M. Bele, M. Kostelec, T. Đukić, N. Van de Velde, I. Jerman, S. Cherevko, N. Hodnik, B. Grenorio, M. Gaberšček, Towards the continuous production of multigram quantities of highly uniform supported metallic nanoparticles and their application for synthesis of superior intermetallic Pt-alloy ORR electrocatalysts, ACS Appl. Energy Mater. 4 (2021) 13819–13829, https://doi.org/10.1021/acsaem.1c02570.
[44] T. Đukić, L. Moriau, L. Pavko, M. Kostelec, M. Prokop, F. Ruiz-Zepeda, M. Šala, G. Dražič, M. Gatalo, N. Hodnik, Understanding the crucial significance of the temperature and potential window on the stability of carbon supported Pt-alloy nanoparticles as oxygen reduction reaction electrocatalysts, ACS Catal 12 (2022) 101–115, https://doi.org/10.1021/acscatal.1c04205.
[45] M. Gatalo, A.M. Bonastre, L. Moriau, H. Burdett, F. Ruiz-Zepeda, E. Hughes, A. Hodgkinson, M. Šala, L. Pavko, M. Bele, N. Hodnik, J. Sharman, M. Gaberšček, Importance of chemical activation and the effect of low operation voltage on the performance of Pt-alloy fuel cell electrocatalysts, ACS Appl. Energy Mater 5 (2022) 8862–8877, https://doi.org/10.1021/acsaem.2c01359.
[46] T. Đukić, L. Pavko, P. Jovanovič, N. Maselj, M. Gatalo, N. Hodnik, Stability challenges of carbon-supported Pt-nanoalloys as fuel cell oxygen reduction reaction electrocatalysts, Chem. Commun. 58 (2022) 13832–13854, https://doi.org/10.1039/D2CC05377B.
[47] S. Cherevko, N. Kulyk, K.J.J. Mayrhofer, Durability of platinum-based fuel cell electrocatalysts: dissolution of bulk and nanoscale platinum, Nano Energy 29 (2016) 275–298, https://doi.org/10.1016/j.nanoen.2016.03.005.
[48] C. Wei, Z. Wang, K. Otani, D. Hochfilzer, K. Zhang, R. Nielsen, I. Chorkendorff, J. Kibsgaard, Benchmarking electrocatalyst stability for acidic oxygen evolution reaction: the crucial role of dissolved ion concentration, ACS Catal 13 (2023) 14058–14069, https://doi.org/10.1021/acscatal.3c03257.
[49] K. Ehelebe, J. Knoppel, M. Bierling, B. Mayerhofer, T. Bohm, N. Kulyk, S. Thiele, K. J.J. Mayrhofer, S. Cherevko, Platinum dissolution in realistic fuel cell catalyst layers, Ang. Int. Ed. Chem. 60 (2021) 8882–8888, https://doi.org/10.1002/anie.202014711.